Detection wavelength of very long wavelength quantum-well infrared photodetector



2003 J. Phys.: Condens. Matter 15 6311

(http://iopscience.iop.org/0953-8984/15/37/001)

INSTITUTE OF PHYSICS PUBLISHING JOURNAL OF PHYSICS: CONDENSED MATTER

J. Phys.: Condens. Matter **15** (2003) 6311–6320 PII: S0953-8984(03)60769-1

# Detection wavelength of very long wavelength quantum-well infrared photodetector

**J Jiang[1], Y Fu[2], Ning Li[1], X S Chen[1], W L Xu[1] and W Lu[1]**

[1] National Laboratory for Infrared Physics, Shanghai Institute of Technical Physics, Chinese Academy of Sciences, 500 Yutian Road, Shanghai 200083, People's Republic of China
[2] Physical Electronics and Photonics, Microtechnology Centre at Chalmers, Department of Microelectronics and Nanoscience, Fysikgränd 3, Chalmers University of Technology, S-412 96 Göteborg, Sweden

Received 9 March 2003, in final form 8 August 2003
Published 8 September 2003
Online at stacks.iop.org/JPhysCM/15/6311

**Abstract**

Based on a detailed discussion of the energy band structure and optical transitions in very long wavelength (∼14 $\mu$m) GaAs/AlGaAs quantum well infrared photodetectors (QWIPs), we have built a practical QWIP model. We have studied various key factors that determine the photogenerated carriers and detection wavelength of very long wavelength QWIPs. Consequently, we have found and confirmed a distinctive difference between the photocurrent of QWIPs with only one confined state in the quantum well (QW) and those binding two confined states, which resulted in a different dependence of the detection wavelength on the QW width. Also, we have discussed the dependence of the response wavelength on several other parameters for very long wavelength QWIPs, such as barrier width and Al mole fraction. Afterwards, a series of very long wavelength QWIP devices have been fabricated and measured, whose photocurrents are well reproduced by our calculation. Based on the theoretical model and experimental data, a simple and convenient polynomial equation has been deduced, using structure parameters of very long wavelength QWIPs to calculate the detection wavelength and offering convenience in device designing.

(Some figures in this article are in colour only in the electronic version)

## 1. Introduction

Infrared detection has been a key factor in the development of infrared technology for more than 40 years. Since 1970, InSb and HgCdTe have been the principal materials for various infrared detector applications. Motivated by smart thermal imaging systems, the format of the infrared detector changed from a single-element device to focal plane arrays (FPAs) in the mid-1980s. Subsequently, long-wavelength detectors have recently become attractive for

  

**Table 1.** Structure parameters of very long wavelength QWIPs. The barrier thickness is 50 nm, $L_W$ is the well width in units of nm, $x$ is the Al mole fraction in the $Al_xGa_{1-x}As$ barrier, the unit of the doping level $N_D$ is $10^{17}$ cm$^{-3}$. $\lambda_p$ and $\lambda_c$ are the photocurrent peak and cut-off wavelengths in units of $\mu$m, while $\lambda_0$ is the theoretical cut-off wavelength. $T$ and $T_B$ are the device operating temperature and the measuring black body temperature in units of K.

| $L_W$ | $x$ | $N_D$ | $\lambda_p$ | $\lambda_c$ | $\lambda_0$ | $T$ | $T_B$ | Reference |
|---|---|---|---|---|---|---|---|---|
| 5 | 0.14 | 3 | 13.2 | 14.9 | 21.7 | 10 | | [9] |
| 4 | 0.16 | 3 | 12 | 14.2 | 22.1 | 10 | | [9] |
| 5 | 0.15 | 5 | 13.3 | 14.7 | 19.7 | 50 | 1000 | [10] |
| 6 | 0.15 | 5 | 13.5 | 14.5 | 17.1 | 300 | 1000 | [10, 11] |
| 6 | 0.15 | 5 | 13.2 | 14.0 | 17.1 | 60 | 1000 | [10, 11] |
| 7 | 0.1 | 3 | 16.6 | 19 | 26.6 | 77 | 1000 | [11] |
| 6 | | 2.5 | 14.5 | 15 | | 77 | | [12] |

a number of sensor applications. However, the technology required for a longer-wavelength HgCdTe detector and a higher mercury concentration have been proven to be rather difficult.

Due to the rapid development of low-dimensional materials, the quantum well infrared photodetector (QWIP) has been developed over the past decade [1–5]. Investigation has been concentrated on the comparison between HgCdTe and QWIP detectors [6–8] and it has been generally concluded that the GaAs/AlGaAs multiple quantum well (MQW) photodetector is very promising for very long wavelength applications. Compared with HgCdTe photodiodes, the GaAs/AlGaAs QWIPs have the advantage in large uniform FPAs, mature III–V technology, high production yield, low cost, high speed, radiation hardness and very long wavelength capability.

Like any other electronic and optoelectronic devices, device modelling has always been an important issue in infrared detector design and fabrication. However, mainly due to the difficulty in ascertaining the real parameters of very long wavelength QWIPs and due to the neglect of the superlattice minibands above the energy barriers in some work, it is noticed that the theoretical design for very long wavelengths has been proven to be unsuccessful until now. Table 1 lists the reported GaAs/AlGaAs QWIP structures and detection wavelengths. Here we see very different QWIP structures, while their detection wavelengths are rather close to each other. The differences between the work of [13, 14] and others are the narrow barrier widths, which form the superlattice minibands in the continuum above the energy barriers [14]. The miniband boundary conditions were applied to understand fine structures in the photocurrent spectra of multiple QWIPs having a detection wavelength of 8 $\mu$m [15].

Here we try to establish a practical very long wavelength GaAs/AlGaAs QWIP model based on real device structures.

## 2. Device structure details

Structures of QWIP devices under consideration are shown schematically in figure 1, which have been applied to three real QWIP devices (samples A, B and C) for experimental verification of our model and calculation. Samples were grown by molecular beam epitaxy on semi-insulating GaAs(100) substrates. The MQW structure consists of 50 periods of an n-type doped GaAs well and a $Al_xGa_{1-x}As$ barrier. The MQW is sandwiched between a 1.8 $\mu$m GaAs top layer and a 0.5 $\mu$m bottom contact layer. Both layers are n-type doped at $2.5 \times 10^{17}$ cm$^{-3}$. The barrier widths of the samples are 60 nm and the well widths are 7.5, 6.9 and 6.4 nm, respectively. Three devices have the same Al mole fraction in the $Al_xGa_{1-x}As$ barrier with $x = 0.14$ from the material MBE growth parameter. Since the Al mole fraction will strongly

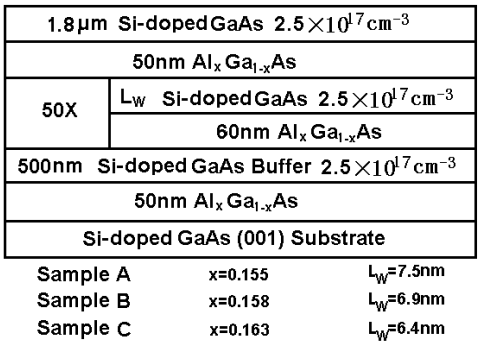


**Figure 1.** Schematic epitaxial layer of the QWIP structure.

affect the response spectrum of very long wavelength QWIPs, the photoluminescence (PL) measurement was used to obtain the real Al mole fraction. Based on both the 80 and 300 K temperature PL spectra, the Al mole fraction of samples are proved to be 0.155, 0.158 and 0.163 for samples A, B and C, respectively.

## 3. Electronic states of QWIP

Let the well width be $L_W$, the barrier thickness $L_B$ and the period $L = L_W + L_B$. We defined the MQW direction as the $z$ axis with the zero point at the centre of the first AlGaAs barrier, the plane perpendicular to this direction as the $xy$ plane. The potential distribution along the $z$ direction can be described as

$$V_B(z) = \begin{cases} 0 & L_B/2 < z - nL < L_B/2 + L_W \\ \Delta & -L_B/2 < z - nL < L_B/2 \end{cases} \tag{1}$$

where $\Delta$ is the barrier potential. Since the Hamiltonian $H$ is translationally symmetric in the $xy$ plane so, with the periodic character along the $z$ direction, the wavefunctions confined in the QW can be written as

$$\psi_{j,k}(\boldsymbol{r}) = \psi_j(z)\mathrm{e}^{\mathrm{i}(k_x x + k_y y)},$$

and the extended states above the QW should be

$$\psi_{j,q}(\boldsymbol{r}) = \psi_j(z)\mathrm{e}^{\mathrm{i}(q_x x + q_y y + q_z z)},$$

where $j = 1, 2, \ldots, N$ is the band index, $\boldsymbol{r}$ is the coordinate in three-dimensional space, $\boldsymbol{k} = (\boldsymbol{k}_x, \boldsymbol{k}_y)$ and $\boldsymbol{q}$ are the wavevectors in the $xy$ plane and three-dimensional space. $\psi_j(z)$ is the envelope function and is normalized in the $z$ direction, which is determined by

$$\left[\frac{-\hbar}{2m^*}\frac{\mathrm{d}^2}{\mathrm{d}z^2} + V_B(z)\right]\psi_j(z) = E_j\psi_j(z) \tag{2}$$

where $m^*$ is the effective mass.

Applying the transfer matrix method, the energy states have been calculated, as shown in table 2. It is found that there are two confined states $\psi_0$ and $\psi_1$ for samples A and B, and only one confined state $\psi_0$ for sample C. The results are numerically consistent with other theoretical consideration, e.g. the complex eigenvalue approach [16–19]. Since the second confined states in sample A and B are much close to the barrier potential, under external bias, carriers in those states can escape and result in a current. Furthermore, the calculation of the

**Table 2.** Calculated energy level in QWIP devices, samples A, B and C, where $\Delta$ is the barrier potential, $E_f$ is the Fermi level, $E_{c1}$ and $E_{c2}$ are the first and second confined states, respectively, and $E_{e1}$ and $E_{e2}$ are the first and second excited states respectively. The experimentally measured and calculated response peak positions are $\lambda_{p,exp}$, $\lambda_{p,cal}$ and FWHM $\Delta\lambda_{exp}$, $\Delta\lambda_{cal}$.

| Sample | A | B | C |
|---|---|---|---|
| $\Delta$ (meV) | 129.6 | 131.7 | 136.0 |
| $E_f$ (meV) | 43.8 | 47.3 | 51.2 |
| $E_{c1}$ (meV) | 40.1 | 44.5 | 49.1 |
| $E_{c2}$ (meV) | 125.9 | 130.9 | —— |
| $E_{e1}$ (meV) | 131.2–132.7 | 133.3–136.3 | 137.6–142.3 |
| $E_{e2}$ (meV) | 135.9–139.6 | 138.1–143.5 | 142.5–149.5 |
| $\lambda_{p,exp}$ ($\mu$m) | 14.6 | 14.1 | 13.6 |
| $\lambda_{p,cal}$ ($\mu$m) | 14.5 | 14.2 | 13.6 |
| $\Delta\lambda_{exp}$ ($\mu$m) | 2.20 | 2.88 | 3.36 |
| $\Delta\lambda_{cal}$ ($\mu$m) | 2.24 | 2.81 | 2.94 |

Fermi level showed that electrons only occupied the first confined state $\psi_0$, which we called the ground state. In fact, the number of confined states is just what we desired before the design, offering the convenience for us to discuss the different behaviour between photocurrents due to carrier transitions from the confined state to confined state and those from the confined state to extended states.

## 4. Calculation of photocurrent

We apply the quantum perturbation theory in the following to discuss the photoexcitation [20]. Then equation (2) can be described by the Hamiltonian $H$:

$$H\psi_i = E_i\psi_i. \tag{3}$$

At a time parameter $t = 0$ a perturbation $H_{ex}e^{-i\omega t}$ is switched on. The wavefunction of the Hamiltonian

$$H + H_{ex}e^{-i\omega t} \tag{4}$$

is expanded in the basis of $\{\psi_i, E_i\}$ in the form of

$$\psi = \sum_i a_i\psi_i e^{-iE_i t/\hbar} \tag{5}$$

so that

$$i\hbar\frac{da_j}{dt} = \sum_i \langle\psi_j|H_{ex}|\psi_i\rangle e^{i\Omega_j t}a_i \tag{6}$$

where $\hbar\Omega_j = E_j - E_i - \hbar\omega$.

Suppose that, before $t = 0$, the electron under investigation occupies the ground state $\psi_0$, i.e. $a_0(t < 0) = 1$ and $a_i(t < 0) = 0$ if $i \neq 0$. By the first-order perturbation theory

$$i\hbar\frac{da_j}{dt} = \langle\psi_j|H_{ex}|\psi_0\rangle e^{i\Omega_j t}. \tag{7}$$

Let

$$H_j \equiv \langle\psi_j|H_{ex}|\psi_0\rangle. \tag{8}$$

Let us introduce the dissipation processes phenomenologically by the concept of a lifetime, $1/\gamma$, of the electron in the excited states. Hence, the unperturbed eigenstate $\psi_j$ becomes

$$\psi_j e^{-(iE_j+\hbar\gamma)t/\hbar} \tag{9}$$

and equation (7) is replaced by

$$i\hbar \frac{da_j}{dt} = H_j e^{-(i\Omega_j+\gamma)t}. \tag{10}$$

At steady state, i.e. $t \to \infty$,

$$a_j = \int_0^\infty \frac{da_j}{dt}\, dt = \frac{H_j}{i\hbar(i\Omega+\gamma)} \tag{11}$$

so that the total transition probability is calculated as

$$|a_j|^2 = \frac{|H_j|^2}{\hbar^2(\Omega_j^2+\gamma^2)}. \tag{12}$$

The validity of the above equation is subjected to the condition that the lifetime of the excited state, $1/\gamma$, is short enough so that the electrons are not able to accumulate in the excited state. Actually, we take a simple approximation of $\hbar\gamma = 6$ meV in the photocurrent calculation process.

For the infrared radiation, we have

$$\begin{aligned} H_{ex} &= \frac{ie\hbar}{m^*}\boldsymbol{A}\cdot\nabla \\ |\boldsymbol{A}|^2 &= \frac{\hbar n_{bb}}{2\epsilon\omega} \end{aligned} \tag{13}$$

where $m^*$ is the electron effective mass and $n_{bb}$ is the photon number density, $\varepsilon$ is the permittivity of the medium under consideration. The matrix element thus becomes

$$H_{j,\boldsymbol{q},\boldsymbol{k}} = \frac{ie\hbar A_z}{m^*}\delta_{q_x,k_x}\delta_{q_y,k_y}\int_{-L/2}^{L/2}\psi_j^*(z)e^{-iq_z z}\frac{d\psi_0(z)}{dz}\,dz \tag{14}$$

where $\boldsymbol{q} \equiv (q_x, q_y, q_z)$ and $\boldsymbol{k} \equiv (k_x, k_y)$. $\delta_{q_x,k_x} = 1$ when $q_x = k_x$; otherwise, it is zero. The basic requirements for an optical transition in QWIPs are: (1) vertical transition in $k_x$ and $k_y$ and (2) normal incident absorption is not possible. Including the unpolarized state of the incident radiation, $|A_z|^2 = \hbar n_{bb}/8\epsilon\omega$ [21].

Thus, the total number of carriers generated by photons of $n_{bb}$ is

$$n_{ph} = \sum_j \int \frac{2d\boldsymbol{q}}{(2\pi)^3}\int \frac{2d\boldsymbol{k}}{(2\pi)^2}\frac{|H_{j,\boldsymbol{q},\boldsymbol{k}}|^2}{\hbar^2(\Omega_{j,\boldsymbol{q},\boldsymbol{k}}^2+\gamma^2)}[f(E_{0,\boldsymbol{k}}) - f(E_{j,\boldsymbol{q}})] \tag{15}$$

where $E_{j,\boldsymbol{q}}$ and $E_{0,\boldsymbol{k}}$ are energies of the states $(j, \boldsymbol{q})$ and $(0, \boldsymbol{k})$, while $f(E)$ is the Fermi distribution function. For the GaAs/AlGaAs system, $E_x = \hbar^2 k_x^2/2m^*$.

Consider a surface area $S_0$ of the MQW system. The total number of electrons in $V_0 \equiv S_0 \times L$ is

$$n_{well} = \sum_i S_0 \int \frac{2dk_x\,dk_y}{(2\pi)^2} f(E_{k_x,k_y,i}, E_f) + V_0 \int \frac{2dk}{(2\pi)^3} f(E_k, E_f) \tag{16}$$

before irradiation, where $f(E, E_f)$ is the Fermi distribution function:

$$f(E, E_f) = \frac{1}{1+\exp\left(\frac{E-E_f}{k_B T}\right)} \tag{17}$$

$n_{well}$ should be equal to the number of donors in the same spatial region, i.e. $L_W N_D$, where $N_D$ is the doping level in the QW. From this we can determine the Fermi level.

As shown in table 2, the ground states in the QW of samples A, B and C are 40.1, 44.5 and 49.1 meV above the GaAs conduction band edge, respectively. However, with a QW doping level of $N_D$ as $2.5 \times 10^{17}$, the Fermi levels are about 43.8, 47.3 and 50.0 meV above the GaAs

conduction band edge at a device working temperature of 77 K for samples A, B and C, which is shown in table 2. Therefore, only the ground state $E_0$ is occupied. Thus it is right to neglect $f(E_{j,q})$ in equation (15). In addition, $\int 2f(E_{0,k})\,\mathrm{d}\boldsymbol{k}/(2\pi)^2$ is the sheet density of carriers in the QW, which is $L_{\mathrm{W}}N_{\mathrm{D}}$. Defining $\eta(\hbar\omega)$ as the ratio of the densities of photoexcited carriers to photons, and with expressions of equations (13) and (14):

$$\eta(\hbar\omega) = \sum_j \frac{ne^2\hbar^3 n_{bb}}{2m^{*2}\epsilon\omega} \int \frac{2\mathrm{d}q_z}{2\pi} \frac{|\int \psi_j^* \mathrm{e}^{-\mathrm{i}q_z z}\,\mathrm{d}\psi_0(z)|^2}{(E_{j,q_z} - E_0 - \hbar\omega)^2 + \gamma^2}. \tag{18}$$

Knowing the density of photogenerated carriers, the photocurrent spectrum is obtained as [19]

$$J_{\hbar\omega} = e\eta(\hbar\omega)\mu F_z \left[1 + \left(\frac{\mu F_z}{v_{\mathrm{s}}}\right)^2\right]^{-1/2} \tag{19}$$

where $v_{\mathrm{s}}$ is the saturation drift velocity ranging over (0.1–5) $\times 10^6$ cm s$^{-1}$, $\mu$ is the low field carrier mobility having a value of 2000 cm$^2$ V$^{-1}$ s$^{-1}$ for n-type AlGaAs QWIPs and $F_z$ is the electric field in the barrier region induced by the external bias.

## 5. Photodetector response discussion

Individual photodetector elements were processed into 200 $\times$ 200 $\mu$m$^2$ area mesa structures using wet chemical etching. Au/AuGeNi ohmic contacts were evaporated on the top and bottom contact layers. To test the infrared response, each chip was packaged in a standard QWIP geometry with a 45° polished face for optical coupling. The whole assembly was mounted in a Dewar for measurements.

Typical photocurrent spectra of three QWIP devices are presented in figure 2, which were obtained by Fourier transform infrared measurements. Spectra were obtained over a certain range of applied voltage while only those at the optimal external bias (−5 V bias) are presented in figure 2 as dots, showing clearly peaks at wavelengths of 14.6, 14.1 and 13.6 $\mu$m for samples A, B and C, respectively.

The full curve in figure 2 shows the calculation of photocurrent spectra for the QWIP structure as samples A, B and C. In order to compare with the experimental results, both the theoretical and experimental data are normalized to their maximum value. The peak response wavelength and full width at half-maximum (FWHM) are listed in table 2. Since the photocurrent spectrum has a non-symmetrical and broad band behaviour, the relative errors of the response peak and FWHM are about 2 and 4%, respectively. Within these errors, we find a good agreement between theory and experiment. However, we also find that the lineshape is still not well matched to each other. This may be caused by the scattering effect in QWIPs. Many scattering effects, like the electron–phonon scattering, impurity–electron scattering, QW width fluctuation scattering and so on, will influence the lineshape of the photocurrent spectra. But in our model, all these scattering effects are approximated by a energy level broadening factor $\hbar\gamma = 6$ meV. This approximation is obviously too simple to explain the complicated scattering effect. But it is a good approximation for the estimation of the photocurrent peak and width value.

From our calculation, it is found that the first excited state is below, at and above the barrier band edge for samples A, B and C, respectively. So these three samples correspond to the so-called bound-to-bound, bound-to-quasi-bound and bound-to-continue transition modes [2]. In order to study the dependence of the response wavelength $\lambda_{\mathrm{p}}$ on the QW structure near the condition of bound-to-quasi-bound, that is the best mode to optimize the QWIP performance, the relation between $\lambda_{\mathrm{p}}$ and QW width for different Al mole fractions has been calculated. Since

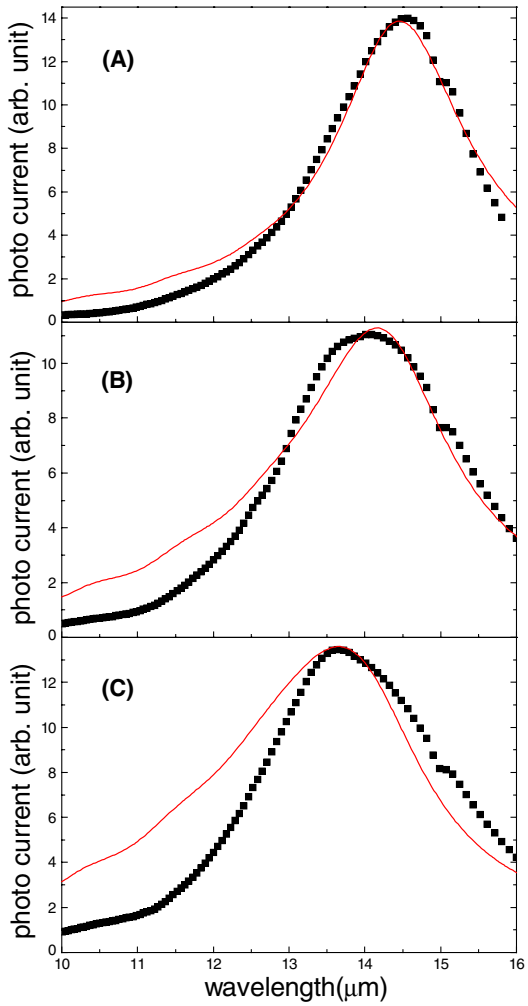


**Figure 2.** (a)–(c) are the photocurrent spectra of devices, samples A, B and C, respectively. All samples are measured at 77 K operating temperature, the square dots represent the experimental results with relative values and full curves represent the calculated photocurrent.

we consider mainly the very long wavelength QWIP device, the Al mole fraction was taken to be in the range from 0.13 to 0.20, while the QW width varies from 4.4 to 9.8 nm. The results are shown in figure 3, from which we can see a U-like dependence of the detection wavelength on the well width for all Al mole fractions. For each line in the figure, devices on the left of the square dot have relatively small well widths and only one confined state in the QW. It is a bound-to-continue operation mode. In this mode, the energy of the ground state will decrease along with the increase in well width. Consequently, the photon energy demanded by the optical transition from the ground state to extended states will increase, resulting in figure 3 in a trend of peak detection wavelength decreasing. There are two confined states for devices on the right side of the square dot on each line. It is a bound-to-bound operation mode. In this mode, the increase in well width leads to the decrease in energy for both confined states. Since the decrease of the excited state is faster than that of the ground confined state, the peak detection wavelength increases with the increase in well width. These effects are confirmed by the

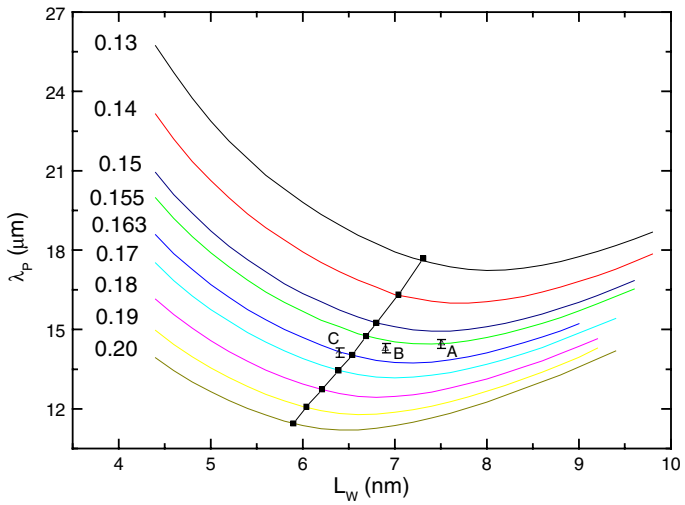


**Figure 3.** Calculated peak detection wavelength $\lambda_p$ as a function of GaAs well width $L_W$ for QWIPs with 60 nm $Al_xGa_{1-x}As$ barrier, $2.5 \times 10^{17}$ cm$^{-3}$ doping level and different Al mole fractions as denoted beside the full curve. The square points indicate the case where the device operates in the bound-to-quasi-bound mode, and the triangular dots indicate the case for QWIP structures as samples A, B and C, where error bars show the error range being 0.2 $\mu$m.

experimental results from samples A, B and C. Their experimental data are shown as triangular point in figure 3. Due to the uncertainties in response peak position determination, here we draw error bars to indicate the range of experimentally measured peak response wavelengths. As we see, they are in good agreement with the theoretical expectation value. Also, the dependence of peak detection wavelength $\lambda_p$ on Al mole fraction can be found in figure 3, which indicates that the larger the Al mole fraction, the shorter the peak detection wavelength.

We have not include in our model the dependence of the response wavelength on well doping level. It is shown in equation (18) that there is no direct correlation between them. It is clear that, based on our simple model, the doping level effect can be neglected. However, the doping level will affect the exchange interaction [22], which will cause a transition energy difference of the order of millielectronvolts. In addition, there exists a direct proportion between the intensity of the photocurrent and well doping level. However, such a judgement is correct only when the doping level is relatively low and the Fermi level of the system is below or close to the ground state in the well.

Meanwhile, a similarity in peak detection wavelength has been found in the calculation of QWIPs with identical parameters except for barrier width. Therefore, it is reasonable to draw a conclusion that, when the barrier width is thick enough (>40 nm), there is not much dependence of peak wavelength on barrier width.

The well width ($L_W$) and Al mole fraction of the barrier ($x$) are the most important parameters in designing the performance. For practical applications, it is useful to have an empirical formula for the relation between response peak $\lambda_p$ and $L_W$, $x$ without making complicated numerical calculations. A simple third-order polynomial equation has been deduced, using both parameters to calculate the detection wavelength of very long wavelength QWIPs:

$$\begin{aligned}
&\lambda_p = P_1 + P_2 \cdot L_W + 1.307\,19 L_W^2 + P_3 \cdot L_W^3 \\
&P1 = 279.8 - 3148x + 15\,078x^2 - 26\,168x^3 \\
&P2 = -45.46 + 482.2x - 2487x^2 + 4592x^3 \\
&P3 = 0.124 - 2.676x + 15.24x^2 - 30x^3.
\end{aligned} \tag{20}$$

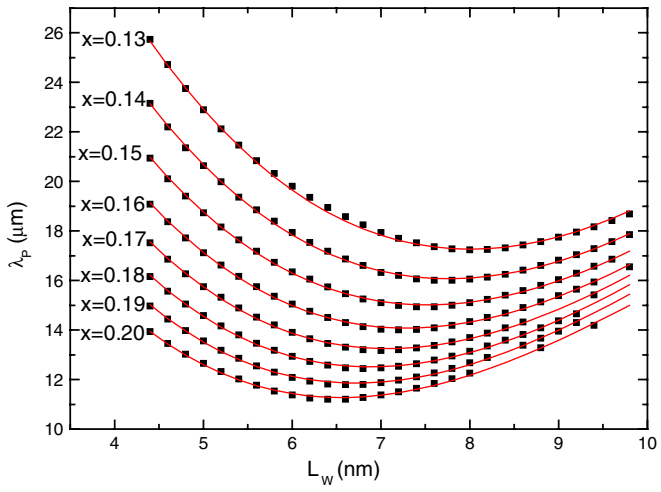


**Figure 4.** Comparing the results of calculated detection wavelength $\lambda_p$ using a polynomial equation and a physical model. Full curve: results of the polynomial equation; dots: results of the physical model. The barrier width of the QWIPs is 60 nm, while the doping level in the QW is $2.5 \times 10^{17}$ cm$^{-3}$.

The result of comparing the calculated detection wavelength using a polynomial equation and the physical model is shown in figure 4. It is clear that they fit very well with each other. Actually, comparing results from our equation (20) and the numerical results from our physical model, the discrepancy is small, with a maximum error 2.1%, minimum error 0.006% and average error 0.6%. Therefore, applying this simple and convenient polynomial equation in the design of very long wavelength QWIPs, we can easily get the detection wavelength, avoiding a repeat of the complicated calculation of energy band structure, the optical coupling process and the optical transition process.

## 6. Conclusion

In summary, we have built a quantum mechanical model for very long wavelength ($\sim$14 $\mu$m) GaAs/AlGaAs QWIPs, which can explain the experimental results of the peak response wavelength. It has also been shown that the peak detection wavelength has a strong dependence on the QW width and Al mole fraction. Moreover, an inverse dependence of peak detection wavelength on QW width between QWIPs operated in a bound-to-bound mode and bound-to-continue mode has been found and verified by experiments. For the convenience of device design, a simple polynomial function has been deduced, using well width and Al mole fraction to calculate the detection wavelength of very long wavelength QWIPs.

## Acknowledgment

This work is financially supported by Chinese National Key Basic Research Special Fund, National Science Foundation of China and One-hundred-person Project of Chinese Academy of Science (no 200012).

## References

[1] Gunapala S D, Bandara S V, Liu J K, Hong W, Sundaram M, Maker P D, Muller R E, Shott C A and Carralejo R 1998 *IEEE Trans. Electron Devices* **45** 1890–5

[2] Levine B F 1993 *J. Appl. Phys.* **74** R1–81

[3] Wan M F *et al* 1998 *J. Infrared Millim. Waves* **17** 76–9
[4] Shen W Z 2000 *Int. J. Infrared Millim. Waves* **21** 1739–46
[5] Li N and Lu W 2000 *J. Infrared Millim. Waves* **19** 25–8
[6] Rogalski A 1997 *Infrared Phys. Technol.* **38** 295–310
[7] Shen S C 1994 *Microelectron. J.* **25** 713–39
[8] Lu W *et al* 1994 *J. Infrared Millim. Waves* **13** 9–13
[9] Zussman A, Levine B F, Hong M and Mannaerts J P 1991 GaAs/$Al_xGa_{1-x}As$ quantum well infrared photodetectors with cutoff wavelength $\lambda_c = 14.9$ $\mu$m *Electron. Lett.* **27** 1512–3
[10] Zussman A, Levine B F, Kuo J M and de Jong J 1991 Extended long-wavelength $\lambda = 11$–$15$ $\mu$m GaAs/$Al_xGa_{1-x}As$ quantum well infrared photodetectors *J. Appl. Phys.* **70** 5101–7
[11] Levine B F, Zussman A, Gunapala S D, Asom M T, Kuo J M and Hobson W S 1992 Photoexcited escape probability, optical gain, and noise in quantum well infrared photodetectors *J. Appl. Phys.* **72** 4429–43
[12] Gunapala S D *et al* 2000 600 × 486 long-wavelength two-color GaAs/AlGaAs quantum well infrared photodetector (QWIP) focal plane array camera *IEEE Trans. Electron Devices* **47** 963–71
[13] Levine B F, Choi K K, Bethea C G, Walker J and Malik R J 1987 New 10 $\mu$m infrared detector using intersubband absorption in resonant tunneling GaAlAs superlattices *Appl. Phys. Lett.* **50** 1092–4
[14] Levine B F, Hasnain G, Bethea C G and Chand N 1989 Broadband 8–12 $\mu$m high-sensitivity GaAs quantum well infrared photodetector *Appl. Phys. Lett.* **54** 2704–6
[15] Fu Y 2001 Boundary conditions of continuum states in characterizing photocurrent of GaAs/AlGaAs quantum well infrared photodetector *Superlattices. Microstruct.* **30** 69–74
[16] Bahder T B, Morrison C A and Bruno H D 1987 Resonant level lifetime in GaAs/AlGaAs doublebarrier structure *Appl. Phys. Lett.* **51** 1089
[17] Bruno J D, Bahder T B and Morrison C A 1988 Limiting response time of double-barrier resonant tunneling structures *Phys. Rev.* B **37** 7098
[18] Zou N, Rammer J and Chao K A 1992 Tunneling escape of electrons from a double-barrier structure *Phys. Rev.* B **46** 15912
[19] Fu Y, Li Ning, Karlsteen M, Willander M, Li Na, Xu W L, Lu W and Shen S C 2000 Thermoexcited and photoexcited carrier transport in a GaAs/AlGaAs quantum well infrared photodetector *J. Appl. Phys.* **87** 511–6
[20] Fu Y, Willander M, Li Ning and Lu W 2002 Quantum mechanical model and simulation of GaAs/AlGaAs infrared photodetector-I Optical aspects *J. Infrared Millim. Waves* **21** 321–6
[21] Fu Y, Willander M, Lu W, Xu W L, Li Ning, Li Na, Liu X Q, Chen Y D and Shen S C 1999 Near-field coupling effect in normal incidence absorption of quantum well infrared photodetectors *J. Appl. Phys.* **85** 1237–9
[22] Hedin L and Lundqvist B I 1971 *J. Phys. C: Solid State Phys.* **4** 2064